

**Combined  $\ell_2$  data and gradient fitting  
in conjunction with  $\ell_1$  regularization**

Nr. 280

Stephan Didas, Simon Setzer, Gabriele Steidl

April, 2006

# Combined $\ell_2$ data and gradient fitting in conjunction with $\ell_1$ regularization

Stephan Didas\*    Simon Setzer†    Gabriele Steidl‡

April 11, 2006

## Abstract

We are interested in minimizing functionals with  $\ell_2$  data and gradient fitting term and (absolute)  $\ell_1$  regularization term with higher order derivatives in a discrete setting. We examine the structure of the solution in 1d by reformulating the original problem into a contact problem which can be solved by dual optimization techniques. The solution turns out to be a discrete polynomial spline whose knots coincide with the contact points. In 2d we modify Chambolle's algorithm to solve the minimization problem with absolute  $\ell_1$  norm and second order derivatives. This requires the application of fast cosine transforms. We demonstrate by numerical denoising examples that the  $\ell_2$  gradient fitting term can be used to avoid both edge blurring and staircasing effects.

*Short title:*  $\ell_1$  regularized gradient fitting

*AMS Subject Classification:* 65K10, 65F22, 65T50, 49M29

*Key words:* higher order  $\ell_1$  regularization, TV regularization, convex optimization, dual optimization methods, discrete splines, splines with defect, G-norm, fast cosine transform, sparse representation.

## 1 Introduction

In image denoising one is interested in removing noise while preserving or even enhancing important structures such as edges. While linear filters typically smooth edges some edge enhancing methods create artificial edges

---

\*didas@mia.uni-saarland.de, Faculty of Mathematics and Computer Science, Saarland University, 66041 Saarbrücken, Germany

†ssetzer@rumms.uni-mannheim.de, University of Mannheim, Institute of Mathematics, D-68131 Mannheim

‡steidl@math.uni-mannheim.de, University of Mannheim, Institute of Mathematics, D-68131 Mannheim

out of continuous gray value transitions. This effect is known as 'staircasing'. In this context, we are concerned with minimizing discrete versions of the functional

$$\frac{1}{2}\|f - u\|_{L_2}^2 + \frac{\alpha}{2}\|\nabla f - \nabla u\|_{L_2}^2 + \beta\| |u^{(\gamma)}| \|_{L_1}, \quad (1)$$

where  $|u^{(\gamma)}|$ ,  $\gamma \in \mathbb{N}_0^2$  denotes the absolute value of appropriate higher order derivatives of  $u$ . For  $|u^{(1,1)}| = |\nabla u|$  and  $\alpha = 0$  the functional (1) is the frequently applied Rudin–Osher–Fatemi (ROF) model [20] which typically shows the staircasing effect. Using higher order derivatives  $\gamma$  one can avoid this effect, see, e.g., [23] but the method tends to introduce some blurring in regions of image edges. To cope with this disadvantage we propose to add an additional gradient fitting term ( $\alpha \neq 0$ ) and examine its influence on the solution. Other possible approaches, e.g., the application of Bregman distances [17] are beyond the scope of this paper.

To get a better idea concerning the structure of the solution of the minimization problem, we first deal with the univariate setting, where the regularization term contains only the  $\ell_1$  norm

$$\frac{1}{2}\|f - u\|_{L_2}^2 + \frac{\alpha}{2}\|f' - u'\|_{L_2}^2 + \beta\|f^{(m)}\|_{L_1}. \quad (2)$$

Again, we focus on the discrete approach with forward differences instead of derivatives. Note that in the continuous setting  $L_1$  regularization in connection with splines was treated in [6] with a careful handling of the non-reflexive space  $L_1$ . In this paper, we reformulate (2) as a contact problem which can be solved via the dual formulation of (2). In case of an additional gradient fitting term ( $\alpha > 0$ ) the computation requires the application of fast discrete cosine transforms. We prove that the solution  $U$  of the contact problem is a discrete polynomial spline of degree  $2m - 1$  with the contact points as spline knots. For  $\alpha = 0$  this spline is 'smooth', i.e., has defect (knot multiplicity) one, see also [24], while for  $\alpha > 0$  it has defect three. The solution  $u$  of (2) is directly determined by the solution  $U$  of the contact problem and appears to be a discrete 'smooth' polynomial spline of order  $m - 1$  with knots related to the contact points. We do not present numerical denoising examples in 1d since they only confirm the 2d findings. For  $\alpha = 0$  and various derivatives  $m$  denoising results are given in [24].

Having examined the structure of the solution in 1d, we turn to our original 2d denoising problem. Here the regularization term includes an *absolute*  $\ell_1$  norm which in contrast to the ordinary  $\ell_1$  norm leads to rotationally invariant solutions. We adapt an algorithm of Chambolle [2] which is also based on the dual version of (1) to our setting. Again we have to apply fast cosine transforms in case of an additional gradient fitting term. The dual algorithms considered so far are based on the fact that the  $\ell_1$  regularization functional is one-homogeneous so that the dual functional is the

indicator function of a convex set. However, in variational image restoration other regularizers, including non-convex ones were also applied. It seems to be interesting to see how the additional gradient fitting term behaves in connection with such penalizers. To this end, we include for numerical comparisons a brief consideration of more general functionals and their numerical solution via the Euler–Lagrange equation and the corresponding reaction–diffusion equation. In our numerical examples we will focus on the non-convex penalizer corresponding to the Perona–Malik diffusivity [18].

This paper is organized as follows: We start with the 1d part in Section 2. First we provide our discrete setting in Subsection 2.1. Then we reformulate the discrete minimization problem as a contact problem and deal with its solution via the dual formulation of the minimization problem in Subsection 2.2. Finally, we examine the structure of the solution both of the contact problem and the original minimization problem in Subsection 2.3.

Section 3 deals with 2d images, where we focus on the practically relevant regularization with at most second order derivatives in the regularization term. After introducing the discrete setting in Subsection 3.1 we turn to the dual formulation and Chambolle’s algorithm in connection with the discrete cosine transform in Subsection 3.2. Subsection 3.3 briefly describes the numerical treatment of regularization functionals which are possibly not one-homogeneous via the corresponding Euler–Lagrange equation. Finally, Subsection 3.4 presents numerical denoising results demonstrating the influence of the additional gradient fitting term.

## 2 Higher order $\ell_1$ regularization in 1d

### 2.1 Discrete setting

In this section, we deal with a discrete version of (2). To this end, let

$$D_{1,N} := \begin{pmatrix} -1 & 1 & 0 & \dots & 0 & 0 & 0 \\ 0 & -1 & 1 & \dots & 0 & 0 & 0 \\ & & & \ddots & \ddots & & \\ 0 & 0 & 0 & \dots & -1 & 1 & 0 \\ 0 & 0 & 0 & \dots & 0 & -1 & 1 \end{pmatrix} \in \mathbb{R}^{N-1,N} \quad (3)$$

be the *first order forward difference matrix* and

$$D_{m,N} := D_{1,N-(m-1)} \cdot \dots \cdot D_{1,N-1} D_{1,N} \in \mathbb{R}^{N-m,N}$$

the *m-th order forward difference matrix*. If the size  $N$  of a difference matrix  $D_{m,N}$  is clear from the context we will skip the second index and write only

$D_m$ . Then it is well known that

$$\begin{aligned}\mathcal{R}(D_{m,N}^T) &= \{f \in \mathbb{R}^N : \sum_{j=1}^N j^r f(j) = 0, r = 0, \dots, m-1\}, \\ \mathcal{N}(D_{m,N}) &= \text{span} \{(j^r)_{j=1}^N : r = 0, \dots, m-1\},\end{aligned}$$

i.e., the range  $\mathcal{R}(D_{n,m}^T)$  of  $D_{n,m}^T$  consists of the vectors with  $m$  vanishing moments while the kernel  $\mathcal{N}(D_{n,m})$  of  $D_{n,m}$  is just given by the discrete polynomials of degree  $\leq m-1$ .

We are interested in minimizing the discrete counterpart of (2)

$$F(u) = \frac{1}{2} \|f - u\|_2^2 + \frac{\alpha}{2} \|D_1 f - D_1 u\|_2^2 + \beta \|D_m u\|_1 \quad (4)$$

which can be rewritten as

$$F(u) = \frac{1}{2} (f - u)^T (I_N + \alpha D_1^T D_1) (f - u) + \beta \|D_m u\|_1. \quad (5)$$

We will see by (21) that the matrix

$$A = A(\alpha) := I_N + \alpha D_1^T D_1$$

is positive definite. Setting  $B^T B := A$  and  $L := D_m$  the functional (5) becomes

$$F(u) = \frac{1}{2} \|B(f - u)\|_2^2 + \beta \|Lu\|_1. \quad (6)$$

The minimizer of (6) can be computed in various ways. In the next subsection, we propose to minimize (6) using its dual formulation. This is closely related to the reformulation of (6) as a contact problem and serves as our basis to gain some insight into the structure of the solution  $u$ .

## 2.2 Contact problem and dual formulation

In this subsection, we focus on minimizing strictly convex functionals of the form

$$F(u) = \frac{1}{2} \|B(f - u)\|_2^2 + \beta \|Lu\|_1, \quad (7)$$

where  $B \in \mathbb{R}^{N,N}$  and  $L \in \mathbb{R}^{N-m,N}$  are arbitrary matrices of full rank. In particular, we are interested in our special setting from the previous subsection.

**Decomposition related to  $\mathcal{N}(L)$ .** Since the regularization term becomes zero if  $u$  is in  $\mathcal{N}(L)$  we want to restrict ourselves to those parts of  $u$  which are in a certain sense orthogonal to  $\mathcal{N}(L)$ . The matrix  $B$  has full rank such that  $A := B^T B$  is positive definite and

$$\langle u, v \rangle_A = \langle Au, v \rangle = v^T Au.$$

defines an inner product on  $\mathbb{R}^N$ . Corresponding to the  $A$  orthogonal decomposition

$$\mathbb{R}^N = \mathcal{N}(L) \oplus_A \mathcal{R}(A^{-1}L^T)$$

every vector  $u \in \mathbb{R}^N$  has a unique decomposition as

$$u = u_0 + u_1, \quad u_0 \in \mathcal{N}(L), \quad u_1 \in \mathcal{R}(A^{-1}L^T). \quad (8)$$

Using this decomposition for  $f$  and  $u$ , we obtain in (7),

$$\begin{aligned} F(u) &= \frac{1}{2} \|B(f_0 - u_0)\|_2^2 + \langle B(f_0 - u_0), B(f_1 - u_1) \rangle + \frac{1}{2} \|B(f_1 - u_1)\|_2^2 \\ &\quad + \beta \|Lu_1\|_1 \\ &= \frac{1}{2} \|B(f_0 - u_0)\|_2^2 + \frac{1}{2} \|B(f_1 - u_1)\|_2^2 + \beta \|Lu_1\|_1. \end{aligned}$$

It is easy to check that  $f_1 = A^{-1}L^TKLf$ , where

$$K := (LA^{-1}L^T)^{-1}.$$

Note that  $K$  exists since  $L$  has full rank. Consequently, to solve (7), we can set  $u_0 := f_0 = f - f_1$  and search for  $u_1 \in \mathcal{R}(A^{-1}L^T)$  minimizing

$$\frac{1}{2} \|B(f_1 - u_1)\|_2^2 + \beta \|Lu_1\|_1.$$

In the following, we assume that  $f \in \mathcal{R}(A^{-1}L^T)$  such that  $f_1 = f$  and  $u_1 = u$ .

**Reformulation as contact problem.** For the solution  $u$  of (7) it is necessary and sufficient that  $0_N$  is an element of the subdifferential  $\partial F(u)$ :

$$0_N \in A(u - f) + \beta L^T \frac{Lu}{|Lu|}, \quad (9)$$

where the quotient is meant componentwise and

$$\frac{x}{|x|} := \begin{cases} 1 & \text{if } x > 0, \\ -1 & \text{if } x < 0, \\ [-1, 1] & \text{if } x = 0. \end{cases}$$

This can be rewritten as

$$\begin{aligned} u &\in f - \beta A^{-1}L^T \frac{Lu}{|Lu|}, \\ Lu &\in Lf - \beta LA^{-1}L^T \frac{Lu}{|Lu|}. \end{aligned} \quad (10)$$

Since  $f, u \in \mathcal{R}(A^{-1}L^T)$  there exist  $F, U \in \mathbb{R}^{N-m}$  such that

$$f = A^{-1}L^T F, \quad u = A^{-1}L^T U. \quad (11)$$

Conversely, we have that

$$F = KLf, \quad U = KLu. \quad (12)$$

Multiplying (10) by  $K$  and using (12) we obtain the inclusion

$$U \in F - \beta \frac{K^{-1}U}{|K^{-1}U|}.$$

Hence (7) can be reformulated as the following **contact problem**:

Find  $U \in \mathbb{R}^{N-m}$  so that

- $\|F - U\|_\infty \leq \beta$ .  
 $U$  lies in a tube around  $F$  of width  $2\beta$ .
- if  $(K^{-1}U)_j > 0$  we have a lower contact point  $U_j = F_j - \beta$ ,  
if  $(K^{-1}U)_j < 0$  we have an upper contact point  $U_j = F_j + \beta$ .

For an illustration of a contact problem see Fig. 1 (right).

To get an idea concerning the structure of  $U$  and  $u$  in the next subsection let us write

$$U = Kc, \quad (13)$$

so that by (11)

$$u = \tilde{K}c, \quad (14)$$

with  $\tilde{K} := A^{-1}L^TK$ . Then the contact problem reads as follows:

Find  $c \in \mathbb{R}^{N-m}$  so that

- $\|F - Kc\|_\infty \leq \beta$ .
- if  $c_j > 0$  we have a lower contact point  $U_j = F_j - \beta$ ,  
if  $c_j < 0$  we have an upper contact point  $U_j = F_j + \beta$ .

Let

$$\Xi := \{j \in \{0, \dots, N-m-1\} : c_j \neq 0\} \quad (15)$$

be the (sub)set of contact point indices. If  $\#\Xi$  is small, then  $c$  becomes sparse and (13) (resp. (14)) are sparse representations of  $U$  (resp.  $u$ ) determined by the corresponding columns of  $K$  (resp.  $\tilde{K}$ ). In the next subsection we will have a closer look at these columns.

In general the solution of the contact problem is not straightforward. Only for the special case that  $B = I_N$  and  $L = D_1$  there exists the so-called 'taut-string' algorithm [4] which is based on a convex hull algorithm and requires only  $\mathcal{O}(N)$  arithmetic operations. Concerning tube algorithms see also [7].

We will solve the problem via the dual approach to (7).

**Dual formulation.** To give the dual formulation of (7) we apply that  $J(u) := \|Lu\|_1$  is one-homogeneous so that its conjugate  $J^*$  is the indicator function of the convex set

$$\mathcal{S}_L := \{v \in \mathcal{R}(L^T) : \langle v, w \rangle \leq J(w) \quad \forall w \in \mathbb{R}^N\}. \quad (16)$$

It is easy to check that

$$\mathcal{S}_L = \{v = L^T V : \|V\|_\infty \leq 1\}. \quad (17)$$

Then the inclusion (9) can be rewritten as

$$\frac{1}{\beta} A(f - u) \in \partial J(u)$$

which is equivalent to

$$u \in \partial J^* \left( \frac{1}{\beta} A(f - u) \right)$$

and with  $v := A(f - u)$ , i.e.,  $u = f - A^{-1}v$  to

$$f - A^{-1}v \in \partial J^* \left( \frac{v}{\beta} \right).$$

Obviously,  $v$  fulfills this inclusion if and only if it minimizes the functional

$$\frac{1}{2} \|Bf - (B^{-1})^T v\|_2^2 + J^* \left( \frac{v}{\beta} \right). \quad (18)$$

By (17) this is the case if and only if  $v = L^T V$  and  $V$  solves the minimization problem

$$\|Bf - (B^{-1})^T L^T V\|_2^2 \rightarrow \min, \quad \text{s.t. } \|V\|_\infty \leq \beta. \quad (19)$$

This is actually a quadratic optimization problem with linear constraints which can be solved by standard optimization techniques. Finally, we obtain

$$u = f - A^{-1} L^T V.$$

Up to now we have not used the decomposition (8) for the solution. To see the relation to the contact problem, we assume again that  $f \in \mathcal{R}(A^{-1}L^T)$ . Then, using (11), we can reformulate (19) as

$$\|(B^{-1})^T L^T U\|_2^2 = \|U\|_{K^{-1}}^2 \rightarrow \min, \quad \text{s.t. } \|F - U\|_\infty \leq \beta \quad (20)$$

and with (13) as

$$c^T K c \rightarrow \min, \quad \text{s.t. } \|F - Kc\|_\infty \leq \beta.$$

Thus, the vector  $U$  in our contact problem solves the minimisation problem (20).

In the following, we are interested in the structure of  $u$  and  $U$  for the special matrices  $B$  and  $L$  from Subsection 2.1.

### 2.3 Spline character of the solution

We want to examine the structure of the solution of our minimization problem for our original setting  $L = D_m$  and

$$A = A(\alpha) = I_N + \alpha D_1^T D_1.$$

To get some intuition Fig. 1 illustrates the solution of (4) and of the corresponding contact problem for the WaveLab signal 'Heavisine' with  $N = 64$  points, see [11] for WaveLab. The solution was computed using the 'quadprog' procedure of the MATLAB optimization toolbox.

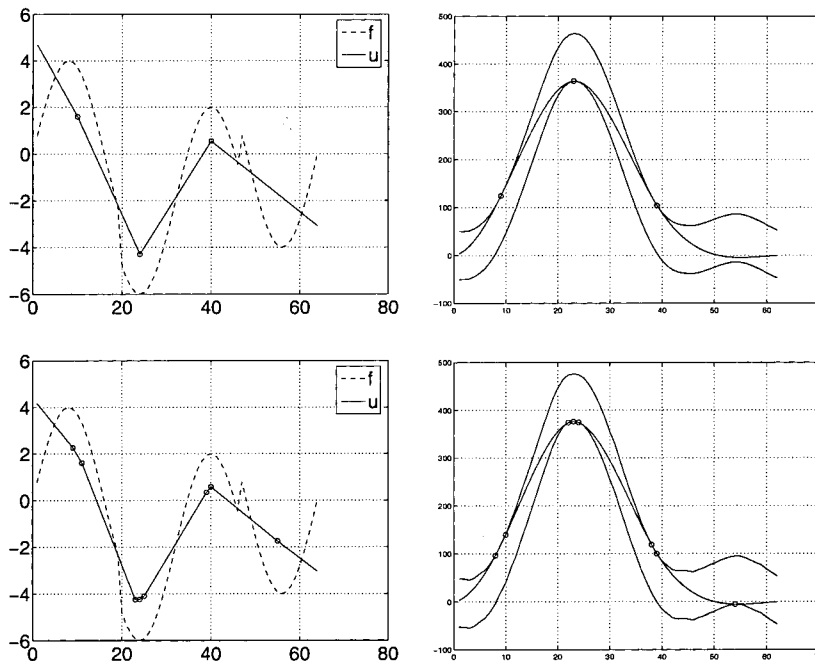


Figure 1: Solutions of the minimization problem (4) and the corresponding contact problem (20) for  $m = 2$  and  $\beta = 50$ . Left: Original signal  $f$  and solutions  $u$  for  $\alpha = 0$  (top) and  $\alpha = 2$  (bottom). Right: Corresponding tubes around  $F$  and solution  $U$  of the contact problem. Here 'o' illustrate the spline knots corresponding contact points.

We will see that  $U$  and  $u$  are discrete polynomial splines of degree  $m - 1$  and  $2m - 1$ , respectively, where  $U$  has some higher defect in case  $\alpha > 0$ . Let us recall the basic spline notation.

**Discrete polynomial splines.** A real-valued function  $s$  defined on  $[a, b]$  is a *polynomial spline of order  $m$  with knots  $a < x_1 < \dots < x_r < b$*  if

$$s^{(m)} = \sum_{k=1}^r c_k \delta(\cdot - x_k),$$

where  $\delta$  denotes the delta-distribution. In other words,  $s$  is a polynomial of degree  $\leq m - 1$  on each interval  $[x_k, x_{k+1}]$ ,  $k = 0, \dots, r$ ;  $x_0 := a$ ,  $x_{r+1} := b$  and  $s \in C^{m-2}[a, b]$ . These smoothest polynomial splines are also called *splines with defect 1* or *with knot multiplicity 1*.

Let  $n := \lfloor m/2 \rfloor$ . Then we can analogously define the *discrete polynomial splines* on  $\{0, \dots, N-1\}$  of order  $m$  with knots  $j_1+n, \dots, j_r+n \in \{n, \dots, N - \lfloor \frac{m}{2} \rfloor\}$  as the vectors  $s \in \mathbb{R}^N$  satisfying

$$D_m s = \sum_{k=1}^r c_{j_k} e_{j_k},$$

where  $e_j \in \mathbb{R}^{N-m}$  denotes the  $j$ -th unit vector. Material on discrete splines can be found, e.g., in [22] and in connection with optimization problems different from the one considered here in [12, 13].

For  $\alpha > 0$ , we have to consider splines with higher defects. A real-valued function  $s$  defined on  $[a, b]$  is a *polynomial spline of order  $m$  with knots  $a < x_1 < \dots < x_r < b$  and defect (knot multiplicity) 3* if

$$s^{(m)} = \sum_{k=1}^r c_k \delta(\cdot - x_k) + c'_k \delta'(\cdot - x_k) + c''_k \delta''(\cdot - x_k).$$

In other words,  $s$  is of lower smoothness, namely  $s \in C^{m-4}[a, b]$ . Here we may restrict our interest to the discrete counterpart of splines with defect 3 satisfying

$$s^{(m)} = \sum_{k=1}^r c_k (\delta(\cdot - x_k) + \alpha \delta''(\cdot - x_k)).$$

We say that  $s \in \mathbb{R}^N$  is a *discrete polynomial spline* on  $\{0, \dots, N-1\}$  of order  $m$  with knots  $j_1+n, \dots, j_r+n \in \{n, \dots, N - \lfloor \frac{m}{2} \rfloor\}$  and  $\alpha$ -defect 3 if  $s$  satisfies

$$D_m s = \sum_{k=1}^r c_{j_k} (e_{j_k} + \alpha e''_{j_k}),$$

where  $e''_j := (0_{j-1}, -1, 2, -1, 0_{N-m-2-j})^T$  for  $j = 1, \dots, N - m - 2$ ,  $e''_0 := (2, -1, 0_{N-m-2})^T$  and  $e''_{N-m-1} := (0_{N-m-2}, -1, 2)^T$ .

**Spline structure of  $u$ .** Based on the sparse representations (13) and (14) of  $U$  and  $u$  it seems to be useful to have a closer look at the matrices  $K$  and  $\tilde{K}$ . First, we verify that for our special case

$$\begin{aligned} K &= K_m(\alpha) = (D_m A(\alpha)^{-1} D_m^T)^{-1}, \\ \tilde{K} &= \tilde{K}_m(\alpha) = A(\alpha)^{-1} D_m^T K_m(\alpha). \end{aligned}$$

Now we see by definition that

$$D_m \tilde{K}_m(\alpha) = I_{N-m}, \quad D_m u = c.$$

Consequently, we obtain the following corollary concerning the structure of  $u$ .

**Corollary 2.1** *The  $k$ -th column of  $\tilde{K}_m(\alpha)$  is a fundamental discrete polynomial spline of order  $m$  with knot  $k+n$ . The solution  $u$  of (7) is a discrete polynomial spline of order  $m$  with knots  $\Xi+n$ , where  $\Xi$  is given by the indices of the contact points (15).*

Fig. 2 illustrates the fundamental splines given by the columns of  $\tilde{K}_m(\alpha)$  for various values of  $m$  and  $\alpha$ .

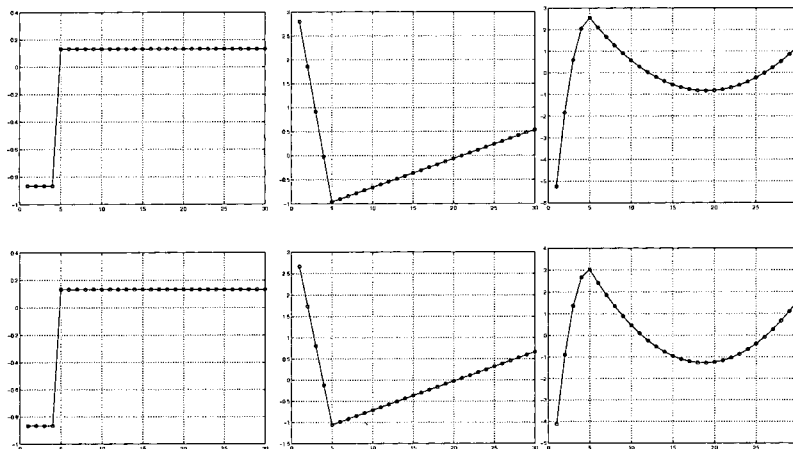


Figure 2: Fourth column of  $\tilde{K}_m(\alpha)$  for  $m = 1, 2, 3$  (left to right) and  $\alpha = 0$  (top),  $\alpha = 10$  (bottom), where  $N = 30$ .

**Spline structure of  $U$ .** To get some insight into the structure of the solution  $U$  of the contact problem, we need some technical preparations. Let

$$T(a) := \begin{pmatrix} a_0 & a_1 & \dots & a_{N-2} & a_{N-1} \\ a_1 & a_0 & \dots & a_{N-3} & a_{N-2} \\ \vdots & \vdots & \ddots & \vdots & \vdots \\ a_{N-2} & a_{N-3} & \dots & a_0 & a_1 \\ a_{N-1} & a_{N-2} & \dots & a_1 & a_0 \end{pmatrix},$$

$$H(a) := \begin{pmatrix} a_0 & a_1 & \dots & a_{N-2} & a_{N-1} \\ a_1 & a_2 & \dots & a_{N-1} & a_{N-2} \\ \vdots & \vdots & \ddots & \vdots & \vdots \\ a_{N-2} & a_{N-1} & \dots & a_2 & a_1 \\ a_{N-1} & a_{N-2} & \dots & a_1 & a_0 \end{pmatrix}$$

be the symmetric Toeplitz matrix and persymmetric Hankel matrix generated by the vector  $a \in \mathbb{R}^N$ . By

$$S_{N-1} := \left(\frac{2}{N}\right)^{1/2} \left(\sin \frac{jk\pi}{N}\right)_{j,k=1}^{N-1} \in \mathbb{R}^{N-1, N-1}$$

we denote the transform matrix of the sine-I transform of length  $N-1$  and by

$$C_N := \left(\frac{2}{N}\right)^{1/2} \left(\varepsilon_j \cos \frac{j(2k+1)\pi}{2N}\right)_{j,k=0}^{N-1} \in \mathbb{R}^{N, N}$$

with  $\varepsilon_0 := 1/\sqrt{2}$  and  $\varepsilon_j := 1$  for  $j \neq 0$  the matrix of the cosine-II transform of length  $N$ , cf. [19]. Both matrices are orthogonal, i.e.,  $S_{N-1} S_{N-1}^T = I_{N-1}$  and  $C_N^T C_N = I_N$ . Moreover, the vector multiplication with  $S_{N-1}$  and  $C_N$  can be realized in an FFT-like manner with only  $\mathcal{O}(N \log N)$  arithmetic operations.

It is well known that these transforms are strongly related to Toeplitz plus Hankel matrices in the following sense, see, e.g., [19]:

**Lemma 2.2** *The following relations hold true*

$$S_{N-1} \operatorname{diag}(d_j)_{j=1}^{N-1} S_{N-1} = T(a_0, \dots, a_{N-2}) - H(a_2, \dots, a_{N-2}, 0, 0),$$

$$C_N^T \operatorname{diag}(d_j)_{j=0}^{N-1} C_N = T(a_0, \dots, a_{N-1}) + H(a_1, \dots, a_{N-1}, 0),$$

where

$$(d_j)_{j=0}^{N-1} = 2 \left(\varepsilon_k^2 \cos \frac{jk\pi}{N}\right)_{j,k=0}^{N-1} (a_0, \dots, a_{N-2}, 0)^T.$$

In particular, it follows by Lemma 2.2 that

$$D_1^T D_1 = T(2, -1, 0_{N-2}) + H(-1, 0_{N-1}) = C_N^T \Lambda^2 C_N,$$

where

$$\Lambda^2 := \operatorname{diag}(\lambda_j^2)_{j=0}^{N-1}, \quad \lambda_j^2 := 2 - 2 \cos \frac{j\pi}{N} = \left(2 \sin \frac{j\pi}{2N}\right)^2.$$

and consequently

$$A(\alpha) = I_N + \alpha D_1^T D_1 = C_N^T (I_N + \alpha \Lambda^2) C_N. \quad (21)$$

We introduce the cutoff matrix

$$R_n := (0_{N-m,n}, I_{N-m}, 0_{N-m,n}) \in \mathbb{R}^{N-m, N-m+2n}.$$

Multiplication of a vector with  $R_n$  cuts off the first and last  $n$  vector components.

**Lemma 2.3** *Let  $b_k := (-1)^k \binom{2m}{m-k}$ ,  $k = 0, \dots, m$  be the coefficients of the  $2m$ -th binomial filter multiplied by  $(-1)^k$ . Let  $\Lambda := \text{diag}(\lambda_j)_{j=0}^{N-1}$ ,  $\tilde{\Lambda} := \text{diag}(\lambda_j)_{j=1}^{N-1}$ , where  $\lambda_j := 2 \sin \frac{j\pi}{2N}$ . Then the following relations hold true:*

$$\begin{aligned} \text{i)} \quad S_{N-1} \tilde{\Lambda}^{2m} S_{N-1} &= T(b_0, \dots, b_m, 0_{N-m-2}) - H(b_2, \dots, b_m, 0_{N-m}), \\ C_N^T \Lambda^{2m} C_N &= T(b_0, \dots, b_m, 0_{N-m-1}) + H(b_1, \dots, b_m, 0_{N-m}). \end{aligned}$$

$$\begin{aligned} \text{ii)} \quad R_n S_{N-1} \tilde{\Lambda}^{2m} S_{N-1} R_n^T &= T(b_0, \dots, b_m, 0_{N-2m-1}), \quad \text{for } m = 2n + 1, \\ R_n C_N^T \Lambda^{2m} C_N R_n^T &= T(b_0, \dots, b_m, 0_{N-2m-1}), \quad \text{for } m = 2n. \end{aligned}$$

**Proof.** i) By Lemma 2.2 we have that

$$T(b_0, \dots, b_m, 0_{N-m-2}) - H(b_2, \dots, b_m, 0_{N-m}) = S_{N-1} \text{diag}(d_j)_{j=1}^{N-1} S_{N-1}$$

where  $d_j := b_0 + 2 \sum_{k=1}^m b_k \cos \frac{jk\pi}{N}$ . It remains to show that

$$b_0 + 2 \sum_{k=1}^m b_k \cos \frac{jk\pi}{N} = \left(2 - 2 \cos \frac{jk\pi}{N}\right)^m, \quad j = 1, \dots, N-1$$

i.e., that

$$b_0 + \sum_{k=1}^m b_k (e^{ix} + e^{-ix}) = (2 - e^{ix} - e^{-ix})^m, \quad x := \frac{j\pi}{N}.$$

This can easily be verified by induction on  $m$ . The second assertion of i) follows in a similar way.

ii) By i) the Hankel matrix summand influences only the first and last  $n$  rows and columns of  $S_{N-1} \tilde{\Lambda}^{2m} S_{N-1}$  and  $C_N^T \Lambda^{2m} C_N$ , respectively. Thus we obtain ii).  $\square$

**Lemma 2.4** Let  $\Lambda$  and  $\tilde{\Lambda}$  be defined as in Lemma 2.3. Then the kernel  $K_m^{-1}(\alpha)$  can be written as

$$K_m^{-1}(\alpha) = \begin{cases} R_n S_{N-1} \frac{\tilde{\Lambda}^{2m}}{I_{N-1} + \alpha \tilde{\Lambda}^2} S_{N-1} R_n^T & \text{for } m = 2n + 1, \\ R_n C_N^T \frac{\Lambda^{2m}}{I_N + \alpha \Lambda^2} C_N R_n^T & \text{for } m = 2n, \end{cases}$$

where the quotient is defined componentwise.

**Proof.** By Lemma 2.3i) it is easy to check that

$$D_{2n, N-1} = (-1)^n R_n S_{N-1} \tilde{\Lambda}^{2n} S_{N-1}, \quad (22)$$

$$D_{2n, N} = (-1)^n R_n C_N^T \Lambda^{2n} C_N. \quad (23)$$

First, let  $m = 2n$ . Then we obtain by (21) and (23) that

$$\begin{aligned} K_m^{-1}(\alpha) &= D_m C_N^T (I_N + \alpha \Lambda^2)^{-1} C_N D_m^T \\ &= R_n C_N^T \frac{\Lambda^{2m}}{I_N + \alpha \Lambda^2} C_N R_n^T. \end{aligned}$$

Assume now that  $m = 2n + 1$ . By (21) we have that

$$K_1^{-1}(\alpha) = D_1 C_N^T (I_N + \alpha \Lambda^2)^{-1} C_N D_1^T.$$

Straightforward computation gives

$$\begin{aligned} D_1 C_N^T &= \left( \frac{2}{N} \right)^{1/2} \left( \varepsilon_j \left( \cos \frac{j(2k+3)\pi}{2N} - \cos \frac{j(2k+1)\pi}{2N} \right) \right)_{k,j=0}^{N-2, N-1} \\ &= \left( \frac{2}{N} \right)^{1/2} \left( -2\varepsilon_j \sin \frac{j(k+1)\pi}{N} \sin \frac{j\pi}{2N} \right)_{k,j=0}^{N-2, N-1} \\ &= -(0_{N-1,1}, S_{N-1}) \Lambda \end{aligned}$$

and consequently

$$\begin{aligned} K_1^{-1}(\alpha) &= (0_{N-1,1}, S_{N-1}) \Lambda (I_N + \alpha \Lambda^2)^{-1} \Lambda (0_{N-1,1}, S_{N-1})^T \\ &= S_{N-1} \frac{\tilde{\Lambda}^2}{I_{N-1} + \alpha \tilde{\Lambda}^2} S_{N-1}. \end{aligned}$$

Using this relation and (22) we obtain

$$\begin{aligned} K_m^{-1}(\alpha) &= D_{m-1, N-1} D_1 (I_N + \alpha \Lambda^2)^{-1} D_1^T D_{m-1, N-1}^T \\ &= R_n S_{N-1} \frac{\tilde{\Lambda}^{2m}}{I_{N-1} + \alpha \tilde{\Lambda}^2} S_{N-1} R_n^T. \end{aligned}$$

This completes the proof.  $\square$

**Theorem 2.5** Let  $z^T$  denote the  $n$ -th row of  $C_N^T \frac{\Lambda^{2m}}{I_{N+\alpha\Lambda^2}} C_N R_n^T K_m(\alpha)$  if  $m = 2n$  and the  $n$ -th row of  $-S_{N-1} \frac{\tilde{\Lambda}^{2m}}{I_{N-1+\alpha\tilde{\Lambda}^2}} S_{N-1} R_n^T K_m(\alpha)$  if  $m = 2n + 1$ . By  $z_{rev}$  we denote the reversed vector  $z$ . Then our kernels  $K_m(\alpha)$  fulfill

$$(-1)^m D_{2m, N+m} \begin{pmatrix} \alpha z^T \\ 0_{m-1, N-m} \\ K_m(\alpha) \\ 0_{m-1, N-m} \\ \alpha z_{rev}^T \end{pmatrix} = T(1 + 2\alpha, -\alpha, 0_{N-m-2}). \quad (24)$$

**Proof.** We restrict our attention to even  $m = 2n$ . The proof for odd  $m = 2n + 1$  follows the same lines. By Lemma 2.3ii) we have that

$$\begin{aligned} T(b_0, \dots, b_m, 0_{N-2m-1}) &= R_n C_N^T \Lambda^{2m} C_N R_n^T \\ &= R_n C_N^T (I_N + \alpha \Lambda^2) C_N C_N^T \frac{\Lambda^{2m}}{I_{N+\alpha\Lambda^2}} C_N R_n^T. \end{aligned}$$

Using Lemma 2.4 and regarding the tridiagonal structure of  $C_N^T (I_N + \alpha \Lambda^2) C_N$  this can be rewritten as

$$\begin{aligned} T(b_0, \dots, b_m, 0_{N-2m-1}) \\ = T(1 + 2\alpha, -\alpha, 0_{N-m-2}) K_m^{-1}(\alpha) - \alpha \begin{pmatrix} a^T \\ 0_{N-m-2, N-m} \\ a_{rev}^T \end{pmatrix}, \end{aligned}$$

where  $a^T$  denotes the  $n$ -th row of  $C_N^T \frac{\Lambda^{2m}}{I_{N+\alpha\Lambda^2}} C_N R_n^T$ . Multiplication with  $K_m(\alpha)$  results in

$$\begin{aligned} T(b_0, \dots, b_m, 0_{N-2m-1}) K_m(\alpha) + \alpha \begin{pmatrix} z^T \\ 0_{N-m-2, N-m} \\ z_{rev}^T \end{pmatrix} \\ = T(1 + 2\alpha, -\alpha, 0_{N-m-2}). \end{aligned}$$

Now we can enlarge  $(-1)^m T(b_0, \dots, b_m, 0_{N-2m-1})$  by  $2m$  rows and columns to  $(-1)^m D_{2m, N+m}$  to obtain

$$\begin{aligned} (-1)^m D_{2m, N+m} \begin{pmatrix} 0_{m, N-m} \\ K_m(\alpha) \\ 0_{m, N-m} \end{pmatrix} + \alpha \begin{pmatrix} z^T \\ 0_{N-m-2, N-m} \\ z_{rev}^T \end{pmatrix} \\ = T(1 + 2\alpha, -\alpha, 0_{N-m-2}). \end{aligned}$$

Since the first coefficient in the Toeplitz matrix  $(-1)^m D_{2m, N+m}$  is equal to 1, this can be rewritten in the form (24).  $\square$

By Theorem 2.5 we have for  $\alpha = 0$  that the  $k$ -th column of  $(0_{N-m, m}, K_m(\alpha), 0_{N-m, m})$  is a discrete polynomial spline of order  $2m$  on  $\{0, \dots, N+m-1\}$  with knot  $m+k$  and  $(0_m^T, U^T, 0_m^T)$  is a discrete polynomial spline of order  $2m$  with knots  $\Xi + m$ .

For arbitrary  $\alpha \geq 0$ , we obtain by Theorem 2.5 the following corollary.

**Corollary 2.6** *Let  $z$  be given as in Theorem 2.5 and let*

$$K_m^{\text{ext}}(\alpha) := \begin{pmatrix} \alpha z^T \\ 0_{m-1, N-m} \\ K_m(\alpha) \\ 0_{m-1, N-m} \\ \alpha z_{\text{rev}}^T \end{pmatrix}, \quad U^{\text{ext}} := \begin{pmatrix} \alpha z^T c \\ 0_{m-1} \\ U \\ 0_{m-1} \\ \alpha z_{\text{rev}} c^T \end{pmatrix}$$

*Then the  $k$ -th column of  $K_m^{\text{ext}}(\alpha)$  is a discrete polynomial spline on  $\{0, \dots, N+m-1\}$  with  $\alpha$ -defect 3 and knot  $m+k$  and  $U^{\text{ext}}$  is a discrete polynomial spline with  $\alpha$ -defect 3 and knots  $\Xi + m$ .*

The fundamental splines given by the columns of the kernel are illustrated in Fig. 3.

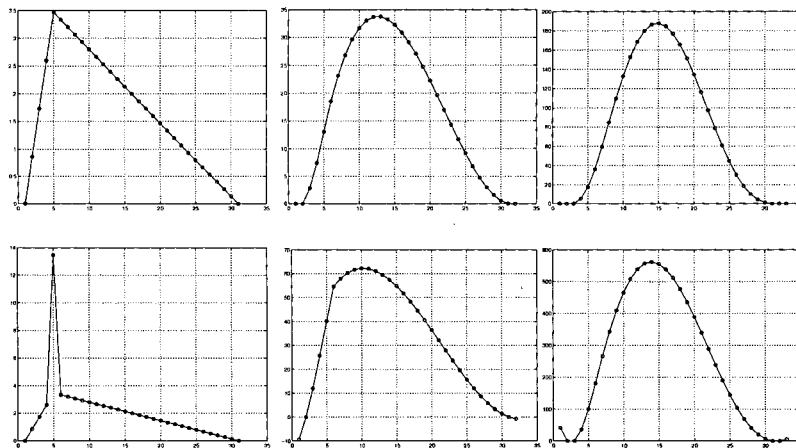


Figure 3: Fourth column of  $K_m^{\text{ext}}(\alpha)$  for  $m = 1, 2, 3$  (left to right) and  $\alpha = 0$  (top),  $\alpha = 10$  (bottom), where  $N = 30$ .

### 3 Second order absolute $\ell_1$ regularization in 2d

#### 3.1 Discrete setting

For simplicity, we restrict our attention to quadratic  $(n, n)$  images and reshape them column by column into a vector  $f$  of length  $N := n^2$ . As discrete counterpart of (1) we are interested in minimizing strictly convex functionals of the form

$$F(u) = \frac{1}{2} \|f - u\|_2^2 + \frac{\alpha}{2} \|\mathcal{D}_1 f - \mathcal{D}_1 u\|_2^2 + \beta \| |\mathcal{D}_m u| \|_1. \quad (25)$$

As in the univariate case,  $\mathcal{D}_1$  will be a discrete partial derivative operator of first order and  $\mathcal{D}_m$  a discrete partial derivative operator of higher order. Here we mainly focus on second order derivatives  $\mathcal{D}_2$ .

In contrast to the univariate case we do not use the  $l_1$  norm in the regularization term but a so-called *absolute  $l_1$*  norm which we introduce next. This guarantees that the solution becomes rotationally invariant. We mention that  $l_1$  norm regularizations without the absolute inner value were treated with respect to first order derivatives in [9] and for second order derivatives in [10]. Fig. 4 illustrates the influence of the rotation invariance.

Let the vectors  $V \in \mathbb{R}^{pN}$ , where  $p, N \in \mathbb{N}$ ,  $p \geq 2$ , and  $|V| \in \mathbb{R}^N$  be given by

$$V = \begin{pmatrix} (V_j^1)_{j=0}^{N-1} \\ \vdots \\ (V_j^p)_{j=0}^{N-1} \end{pmatrix}, \quad |V| = (\|(V_j^r)_{r=1}^p\|_2)_{j=0}^{N-1}.$$

Then, by Lemma A.1,

$$\| |V| \|_1 = \sum_{j=0}^{N-1} |V|_j, \quad \| |V| \|_\infty = \max_{j=0, \dots, N-1} |V|_j \quad (26)$$

are dual norms on  $\mathbb{R}^{pN}$ . For given  $p$ , we call  $\| |V| \|_1$  the *absolute  $l_1$  norm* of  $V$ .

We introduce the partial difference matrices  $\mathcal{D}_1, \mathcal{D}_2$  using the Kronecker product notation. To this end, we use the difference matrix  $D_1 = D_{1,n}$  defined by (3) and set

$$\mathcal{D}_1 := \begin{pmatrix} I_n \otimes \tilde{D}_1 \\ \tilde{D}_1 \otimes I_n \end{pmatrix} \in \mathbb{R}^{2N, N}, \quad \tilde{D}_1 := \begin{pmatrix} D_1 \\ 0_{1,n} \end{pmatrix}.$$

The multiplication with  $\mathcal{D}_1$  mimics just a discrete gradient operator, where the upper  $N$  rows correspond to the derivation in  $x$  direction and the lower  $N$  rows to the derivation in  $y$  direction. Moreover,  $|\mathcal{D}_1 f|$  is a discrete version

of the absolute value of the gradient  $|\nabla f| = (f_x^2 + f_y^2)^{1/2}$ . For a more sophisticated discretization of  $|\nabla f|$  see, e.g., [26]. Further, let

$$\mathcal{D}_2 = \mathcal{D}_2(\epsilon) := \begin{pmatrix} I_n \otimes D_1^T D_1 \\ D_1^T D_1 \otimes I_n \\ \epsilon (\tilde{D}_1^T \otimes \tilde{D}_1) \\ \epsilon (\tilde{D}_1 \otimes \tilde{D}_1) \end{pmatrix}, \quad \epsilon \in \{0, 1\}.$$

be our discrete version of the second order partial derivative operators  $\partial_{xx}$ ,  $\partial_{yy}$ ,  $\partial_{yx}$ ,  $\partial_{xy}$  (top rows to bottom rows), where the mixed derivatives only appear in case  $\epsilon = 1$ . Note that  $D_1^T D_1 = \tilde{D}_1^T \tilde{D}_1$ . Then we see that  $|\mathcal{D}_2 f|$  is the discrete version of the Frobenius norm of the weighted Hessian

$$\nabla^2 f := \begin{pmatrix} f_{xx} & \epsilon f_{xy} \\ \epsilon f_{yx} & f_{yy} \end{pmatrix}.$$

For a variational method including the Hessian see also [8]. Of course other discretizations of second order derivatives are possible and sometimes also necessary, for example if integral identities have to be preserved, see, e.g., [28].

The functional (25) can be rewritten for  $m = 1, 2$  as

$$F(u) = \frac{1}{2} \|B(f - u)\|_2^2 + \beta \| |Lu| \|_1 \quad (27)$$

with  $L \in \{\mathcal{D}_1, \mathcal{D}_2\}$  and  $A = B^T B$ ,

$$A = A(\alpha) := I_N + \alpha \mathcal{D}_1^T \mathcal{D}_1.$$

The matrix  $\mathcal{D}_1^T \mathcal{D}_1$  is just the central difference discretization of the Laplacian with Neumann boundary conditions which can be diagonalized by Kronecker products of the cosine transform matrices  $C_n$ . More precisely, we obtain that

$$A(\alpha) = (C_n \otimes C_n)^T (I_N + \alpha \Lambda_2^2) (C_n \otimes C_n) \quad (28)$$

with  $\Lambda_2^2 = \Lambda^2 \otimes I_n + I_n \otimes \Lambda^2$ ,  $\Lambda := \text{diag} \left( 2 \sin \frac{j\pi}{2n} \right)_{j=0}^{n-1}$ .

### 3.2 Dual formulation

Since  $J(u) := \| |Lu| \|_1$  is one-homogeneous the functional (27) can be minimized as in 1D by switching to the dual minimization problem

$$\frac{1}{2} \|Bf - (B^{-1})^T v\|_2^2 + J^* \left( \frac{v}{\beta} \right) \rightarrow \min, \quad (29)$$

where  $J^*$  is again the indicator function of the set

$$\mathcal{S}_L := \{v \in \mathcal{R}(L^T) : \langle v, w \rangle \leq J(w) \quad \forall w \in \mathbb{R}^N\}, \quad (30)$$

cf. (16) and  $u$  is related to  $v$  by  $u = f - A^{-1}v$ . By Lemma A.2 this set is also given by

$$\mathcal{S}_L = \{v \in \mathcal{R}(L^T) : \min_{v=L^T V} \| |V| \|_\infty \leq 1\}. \quad (31)$$

For  $L := \mathcal{D}_1$ , the norm  $\|v\|_G := \min_{v=L^T V} \| |V| \|_\infty$  is just a discrete version of Meyer's  $G$ -norm which is known as dual norm of the BV norm on the closed subspace  $\mathcal{BV}$  of functions of bounded variation with gradient in  $L_1$ . Concerning higher order derivatives and  $G$ -norm see also [16].

With  $v := L^T V$  problem (29) is equivalent to

$$\|Bf - (B^{-1})^T L^T V\|_2^2 \rightarrow \min, \quad \text{s.t. } \| |V| \|_\infty \leq \beta.$$

This is a quadratic minimization problem with quadratic constraints (if squared). The problem can be solved for example by an algorithm proposed by Chambolle [2]. For our setting with  $L = \mathcal{D}_2$ , this algorithm reads as follows:

**Algorithm.**

*Input:*  $u^{(0)} := f$  and  $V^{(0)} := 0_{4N}$ .

Repeat for  $k = 0$  until a stopping criterion is reached

$$\begin{aligned} W^{(k)} &:= \mathcal{D}_2 u^{(k)} \\ |W^{(k)}| &:= \left( \sum_{r=1}^4 W_r^{(k)} \circ W_r^{(k)} \right)^{1/2} \\ V^{(k+1)} &:= \left( 1_{4N} + \frac{\tau}{\beta} \left( 1_4 \otimes |W^{(k)}| \right) \right)^{-1} \circ \left( V^{(k)} + \tau W^{(k)} \right) \\ u^{(k+1)} &:= f - A^{-1} \mathcal{D}_2^T V^{(k)} \\ k &:= k + 1, \end{aligned}$$

where the inverse is taken componentwise and  $\circ$  denotes the componentwise vector product.

*Output:*  $u := u^{(k+1)}$ .

Chambolle proved that  $u^{(k)}$  converges to the solution  $u$  if

$$\tau \leq 1 / \|(B^{-1})^T L^T\|_2^2 = 1 / \|LA^{-1}L^T\|_2.$$

Now we have obviously that  $\|A^{-1}\|_2 \leq 1$ ,  $\|\mathcal{D}_1\|_2^2 = 8$  and  $\|\mathcal{D}_2(0)\|_2^2 \leq 32$ . Further, we see by applying Gerschgorin's theorem that  $\|\mathcal{D}_2(1)\|_2^2 \leq 64$ . Hence we have to choose

$$\tau \leq \begin{cases} 1/8 & \text{for } L = \mathcal{D}_1, \\ 1/32 & \text{for } L = \mathcal{D}_2(0), \\ 1/64 & \text{for } L = \mathcal{D}_2(1). \end{cases}$$

For computational purposes it is useful to rewrite the Kronecker product notation in the algorithm regarding the following relation: if  $F$  is the original image,  $f$  the corresponding column vector and  $R, S$  are matrices of appropriate sizes, then

$$(R \otimes S)f = S F R^T.$$

Then, using (28), the algorithm can be rewritten as follows:

**Algorithm.**

*Input:*  $u^{(0)} := f$  and  $V_r^{(0)} := 0_N$ ,  $r = 1, \dots, 4$ .

Repeat for  $k = 0$  until a stopping criterion is reached

$$\begin{aligned} W_1^{(k)} &:= D_1^T D_1 u^{(k)} \\ W_2^{(k)} &:= u^{(k)} D_1^T D_1 \\ W_3^{(k)} &:= \tilde{D}_1 u^{(k)} \tilde{D}_1 \\ W_4^{(k)} &:= \tilde{D}_1^T u^{(k)} \tilde{D}_1^T \\ |W^{(k)}| &:= \sum_{r=1}^4 \left( W_r^{(k)} \circ W_r^{(k)} \right)^{1/2} \\ V_r^{(k+1)} &:= \left( 1_N + \frac{\tau}{\beta} \left( 1_4 \otimes |W^{(k)}| \right) \right)^{-1} \circ \left( V_r^{(k)} + \tau W_r^{(k)} \right), \quad r = 1, \dots, 4 \\ x^{(k+1)} &:= D_1^T D_1 V_1^{(k)} + V_2^{(k)} D_1^T D_1 + \tilde{D}_1^T V_3^{(k)} \tilde{D}_1^T + \tilde{D}_1 V_4^{(k)} \tilde{D}_1 \\ u^{(k+1)} &:= f - C_n^T \left( \frac{1}{I_n + \alpha \Lambda_2^2} \circ (C_n x^{(k+1)} C_n^T) \right) C_n, \\ k &:= k + 1, \end{aligned}$$

where the inverses is taken componentwise.

*Output:*  $u := u^{(k+1)}$ .

Since the difference matrices are sparse and the vector multiplication with  $C_n$  can be performed in  $\mathcal{O}(n \log n)$  arithmetic operations, one step of the algorithm requires only  $\mathcal{O}(n^2 \log n)$  arithmetic operations.

### 3.3 Regularization with more general cost functions

Up to now we have considered convex functionals with one-homogeneous regularization terms. However, besides the  $\ell_1$  regularization term it is very common to use other penaliser functions in variational image restoration methods [25, 15, 3, 21]. We are interested to see at least numerically how other regularizers, in particular non-convex ones, behave in conjunction with  $\ell_2$  data and gradient fitting terms.

Here we consider a functional similar to (1), namely

$$E(u) = \int_{\Omega} \left( \frac{1}{2} (f - u)^2 + \frac{\alpha}{2} (\nabla f - \nabla u)^2 + \beta \varphi (\|H(u)\|_F^2) \right) dx \quad (32)$$

where  $\|H(u)\|_F^2 = u_{xx}^2 + u_{xy}^2 + u_{yx}^2 + u_{yy}^2$  is the sum of all squared partial derivatives of order 2. To form the corresponding Euler–Lagrange equation we assume that the penalizer  $\varphi$  is differentiable. In contrast to the previous methods, the  $\ell_1$  norm can only be used as penalizer in an approximate, differentiable version  $\varphi(s^2) = \sqrt{\varepsilon^2 + s^2}$  with a small additional regularization parameter  $\varepsilon$ , cf. [1]. On the other hand, non-convex penalizers like  $\varphi(s^2) = \lambda^2 \ln\left(1 + \frac{s^2}{\lambda^2}\right)$  can be involved. This penalizer is closely related to nonlinear diffusion methods with a diffusivity  $1/(1 + s^2/\lambda^2)$  proposed by Perona and Malik [18]. While the absence of convexity rises theoretical problems, penalizers of this type allow for interesting practical properties, for example enhancement of image features [5].

Under the assumption of sufficient smoothness of  $u$  we can write the Euler-Lagrange equation corresponding to (32) as

$$0 = u - f - \alpha \Delta(u - f) + \partial_{xx} (\varphi'(\|H(u)\|_F^2) u_{xx}) + 2\partial_{xy} (\varphi'(\|H(u)\|_F^2) u_{xy}) + \partial_{yy} (\varphi'(\|H(u)\|_F^2) u_{yy}) . \quad (33)$$

To solve this equation numerically, we introduce an artificial time variable  $t$  and use the initial data  $u(\cdot, 0) = f$  as starting point. Then we understand the solution of (33) as the steady state of the higher order diffusion-reaction equation

$$u_t = u - f - \alpha \Delta(u - f) + \partial_{xx} (\varphi'(\|H(u)\|_F^2) u_{xx}) + 2\partial_{xy} (\varphi'(\|H(u)\|_F^2) u_{xy}) + \partial_{yy} (\varphi'(\|H(u)\|_F^2) u_{yy}) , \quad (34)$$

where we impose natural boundary conditions. For our numerical examples we have discretized this equation with finite differences in the space variable as described above combined with a simple Euler forward scheme in the time variable.

### 3.4 Numerical examples

In this section, we present some numerical examples for the denoising of grey value images in 2d. Since for a human observer as well as for some computer vision systems edges are a very important source of information in an image, one of the major goals of denoising algorithms is to preserve or even enhance edges. In practice especially edge enhancement can lead to the creation of artificial edges out of continuous grey value transitions. This so-called staircasing effect is one of the most prominent shortcomings of many well-established image denoising algorithms, e.g., the ROF model. It creates an oversegmentation of the image into artificial parts. To avoid these artifacts one can involve higher order derivatives into the model which would prefer not only piecewise constant, but also piecewise linear results [27, 10]. Unfortunately, these higher derivative methods tend to introduce some blurring in the region of the image edges.

The main reason for introducing the additional gradient fitting term consists in avoiding the staircasing effect on the one hand and on the preservation of edges and discontinuities on the other hand. Image edges can be characterised as regions where the gradient is high. Thus the gradient fitting term is intended to force the solution to be similar to the initial image especially near edges.

In our experiments we assume an additive noise model: Let  $f \in \mathbb{R}^{n \times n}$  be a noisy version of the initial image  $g \in \mathbb{R}^{n \times n}$ , degraded with additive noise  $\eta$ , i. e.  $f_{ij} = g_{ij} + \eta_{ij}$ . As a quality measure we now use the Signal-to-Noise Ratio defined as

$$\text{SNR}(f, g) := 10 \log_{10} \left( \frac{\sum_{i,j=1}^n (g_{ij} - \mu)^2}{\sum_{i,j=1}^n (f_{ij} - g_{ij})^2} \right),$$

where  $\mu := \frac{1}{n^2} \sum_{i,j=1}^n g_{ij}$  denotes the mean value of  $g$ . The SNR is a widely used measure in image processing and essentially gives the same information as an  $\ell_2$  distance.

The Chambolle-like algorithms were implemented in MATLAB, while the diffusion-reaction approach (34) was implemented in C.

Fig. 5 displays the test image used for the 2d experiment. Table 1 shows the parameters and the error measures of the resulting images. Sections of the results are displayed in Fig. 6. Here TV2 denotes the approach (25); DR stands for the diffusion-reaction type equation (34) with the non-convex penaliser  $\varphi(s^2) = \lambda^2 \ln \left( 1 + \frac{s^2}{\lambda^2} \right)$  and  $\lambda = 1.0$ . The error measures show that adding a gradient fitting term to variational denoising with second-order derivatives enables us to improve the results. Further we notice that the non-convex penalizer can also lead to improvements in practical examples. The resulting images in Fig. 6 give a similar impression. While the ROF model leads to staircasing artifacts, the pure second order methods suffer from blurred edges. The additional gradient fitting can help to avoid both types of problems. We mention that the whole  $256 \times 256$  image related to the depicted part in the middle left of Fig. 6 looks more cloudy than the whole image belonging to the bottom left part. Moreover it should be noted that some noise pixels survive in the image at the bottom right.

## A Appendix

**Lemma A.1** *The norms  $\|\cdot\|_1$  and  $\|\cdot\|_\infty$  defined by (26) are dual norms on  $\mathbb{R}^{pN}$ .*

**Proof.** By applying the Schwarz inequality to  $(V_j^r)_{r=1}^p, (V_j^r)_{r=1}^p$  for  $j = 0, \dots, N-1$  we obtain

$$|\langle V', V \rangle| \leq \langle |V'|, |V| \rangle,$$

	$m$	$\alpha$	$\beta$	SNR	$\ u - f\ _1 \cdot 10^{-5}$
Noisy image	-	-	-	11.16	10.00
ROF	1	-	50	22.74	2.08
TV2	2	0	20	22.15	1.77
TV2	2	0	50	19.92	1.97
TV2	2	1.2	50	22.98	1.74
DR	2	1	1000	24.78	1.59

Table 1: Denoising experiment in 2d: Parameters and error measures.

where equality arises if  $V = (I_p \otimes D)V'$  with some diagonal matrix  $D \in \mathbb{R}^{N,N}$ . Further, we have

$$\langle |V'|, |V| \rangle \leq \| |V'| \|_\infty \| |V| \|_1,$$

where equality arises for  $|V| = c(\delta_{j_0,j})_{j=0}^{N-1}$  with some constant  $c \in \mathbb{R}$  and an index  $j_0$  with  $|V'|_{j_0} := \max\{|V'|_j : j = 0, \dots, N-1\}$ . To get equality in both estimates we may set  $D := \text{diag}(\delta_{j_0,j})_{j=0}^{N-1}$ .  $\square$

Of course, the lemma can be extended to arbitrary  $l_p$ - $l_q$  norms with  $\frac{1}{p} + \frac{1}{q} = 1$ ,  $1 \leq p, q \leq \infty$ . By the following lemma, we see that the sets in (30) and (31) are equivalent.

**Lemma A.2** *Let  $L \in \mathbb{R}^{pN,N}$ . Then*

$$\sup_{w \in \mathbb{R}^N} \frac{|\langle V', Lw \rangle|}{\| |Lw| \|_1} = \min_{L^T U = L^T V'} \| |U| \|_\infty.$$

**Proof.** Let  $\nu := \sup_{w \in \mathbb{R}^N} \frac{|\langle V', Lw \rangle|}{\| |Lw| \|_1}$ . Then we obtain by the same considerations as in the proof of Lemma A.1 and since  $|\langle V', Lw \rangle| = |\langle L^T V', w \rangle| = |\langle U, Lw \rangle|$  for all  $U \in \mathbb{R}^{pN}$  with  $L^T V' = L^T U$  and all  $w \in \mathbb{R}^N$  that

$$\nu \leq \min_{L^T U = L^T V'} \| |U| \|_\infty. \quad (35)$$

To show the reverse direction we consider the subspace  $\mathcal{B} := \mathcal{R}(L)$  of  $\mathbb{R}^{pN}$  equipped with the norm  $\| | \cdot \|_1$ . The mapping  $l_{V'}(Lw) := \langle V', Lw \rangle$  is a linear functional on  $\mathcal{B}$  which has exactly the norm  $\nu$ . By the Hahn-Banach Theorem this functional can be extended to a linear functional  $l$  on  $(\mathbb{R}^{pN}, \| | \cdot \|_1)$  with  $\| | l \| = \| | l_{V'} \|$ . Consequently, there exists  $\tilde{V} \in \mathbb{R}^{pN}$  such that  $l(V) = \langle \tilde{V}, V \rangle$  for all  $V \in \mathbb{R}^{pN}$  and

$$\langle \tilde{V}, Lw \rangle = \langle V', Lw \rangle \quad \forall w \in \mathbb{R}^N.$$

Since this can be rewritten as

$$\langle L^T \tilde{V}, w \rangle = \langle L^T V', w \rangle \quad \forall w \in \mathbb{R}^N$$

the vector  $\tilde{V}$  must fulfil  $L^T \tilde{V} = L^T V'$ . By Lemma A.1 we see that

$$\|l_{V'}\| = \|l\| = \|\tilde{V}\|_{\infty}.$$

Together with (35) this yields the assertion.  $\square$

**Acknowledgements.** This work has been partially funded by the *Deutsche Forschungsgemeinschaft* (DFG).

## References

- [1] R. Acar and C. R. Vogel. Analysis of bounded variation penalty methods for ill-posed problems. *Inverse Problems*, 10:1217–1229, 1994.
- [2] A. Chambolle. An algorithm for total variation minimization and applications. *Journal of Mathematical Imaging and Vision*, (20):89–97, 2004.
- [3] P. Charbonnier, L. Blanc-Féraud, G. Aubert, and M. Barlaud. Two deterministic half-quadratic regularization algorithms for computed imaging. In *Proc. 1994 IEEE International Conference on Image Processing*, volume 2, pages 168–172, Austin, TX, Nov. 1994. IEEE Computer Society Press.
- [4] P. L. Davies and A. Kovac. Local extremes, runs, strings and multiresolution. *Annals of Statistics*, 29:1–65, 2001.
- [5] S. Didas, J. Weickert, and B. Burgeth. Stability and local feature enhancement of higher order nonlinear diffusion filtering. In W. Kropatsch, R. Sablatnig, and A. Hanbury, editors, *Pattern Recognition*, volume 3663 of *Lecture Notes in Computer Science*, pages 451–458. Springer, Berlin, 2005.
- [6] S. D. Fisher and J. W. Jerome. Spline solutions to  $l_1$  extremal problems in one and several variables. *Journal of Approximation Theory*, 13:73–83, 1975.
- [7] W. Hinterberger, M. Hintermüller, K. Kunisch, M. von Oehsen, and O. Scherzer. Tube methods for BV regularization. *Journal of Mathematical Imaging and Vision*, 19:223 – 238, 2003.
- [8] W. Hinterberger and O. Scherzer. Variational methods on the space of functions of bounded Hessian for convexification and denoising. Technical report, University of Innsbruck, Austria, 2003.

- [9] W. Hintermüller and K. Kunisch. Total bounded variation regularization as a bilaterally constrained optimization problem. *SIAM Journal on Applied Mathematics*, 64(4):1311–1333, May 2004.
- [10] M. Lysaker, A. Lundervold, and X. Tai. Noise removal using fourth-order partial differential equations with applications to medical magnetic resonance images in space and time. *IEEE Transactions on Image Processing*, 12(12):1579 – 1590, 2003.
- [11] S. Mallat. *A Wavelet Tour of Signal Processing*. Academic Press, San Diego, second edition, 1999.
- [12] O. L. Mangasarian and L. L. Schumaker. Discrete splines via mathematical programming. *SIAM Journal on Control*, 9(2):174–183, 1971.
- [13] O. L. Mangasarian and L. L. Schumaker. Best summation formulae and discrete splines via mathematical programming. *SIAM Journal on Numerical Analysis*, 10(3):448–459, 1973.
- [14] S. Mehrotra. On the implementation of a primal-dual interior point method. *SIAM Journal on Optimization*, 2(4):575–601, 1992.
- [15] N. Nordström. Biased anisotropic diffusion – a unified regularization and diffusion approach to edge detection. *Image and Vision Computing*, 8:318–327, 1990.
- [16] A. Obereder, S. Osher, and O. Scherzer. On the use of dual norms in bounded variation type regularization. Technical report, Department of Computer Science, University of Innsbruck, Austria, 2004.
- [17] S. Osher, M. Burger, D. Goldfarb, J. Xu, and W. Yin. An iterative regularization method for the total variation based image restoration. *Multiscale Modeling and Simulation*, 4:460–489, 2005.
- [18] P. Perona and J. Malik. Scale space and edge detection using anisotropic diffusion. *IEEE Transactions on Pattern Analysis and Machine Intelligence*, 12:629–639, 1990.
- [19] D. Potts and G. Steidl. Optimal trigonometric preconditioners for nonsymmetric Toeplitz systems. *Linear Algebra and its Applications*, 281:265–292, 1998.
- [20] L. I. Rudin, S. Osher, and E. Fatemi. Nonlinear total variation based noise removal algorithms. *Physica D*, 60:259–268, 1992.
- [21] O. Scherzer. Denoising with higher order derivatives of bounded variation and an application to parameter estimation. *Computing*, 60:1–27, 1998.

- [22] L. L. Schumaker. *Spline Functions: Basic Theory*. Wiley and Sons, New York, 1981.
- [23] G. Steidl. A note on the dual treatment of higher order regularization functionals. *Computing*, 76:135–148, 2005.
- [24] G. Steidl, S. Didas, and J. Neumann. Splines in higher order tv regularization. *International Journal of Computer Vision*, to appear, 2006.
- [25] A. N. Tikhonov. Solution of incorrectly formulated problems and the regularization method. *Soviet Mathematics Doklady*, 4:1035–1038, 1963.
- [26] M. Welk, G. Steidl, and J. Weickert. Locally analytic schemes: A link between diffusion filtering and wavelet shrinkage. Technical report, IMA Preprint, University of Minnesota, 2006.
- [27] Y.-L. You and M. Kaveh. Fourth-order partial differential equations for noise removal. *IEEE Transactions on Image Processing*, 9(10):1723–1730, 2000.
- [28] J. Yuan, C. Schnörr, G. Steidl, and F. Becker. A study of non-smooth convex flow decomposition. In *Proc. Variational, Geometric and Level Set Methods in Computer Vision*, volume 3752 of *LNCS*, pages 1–12. Springer, 2005.

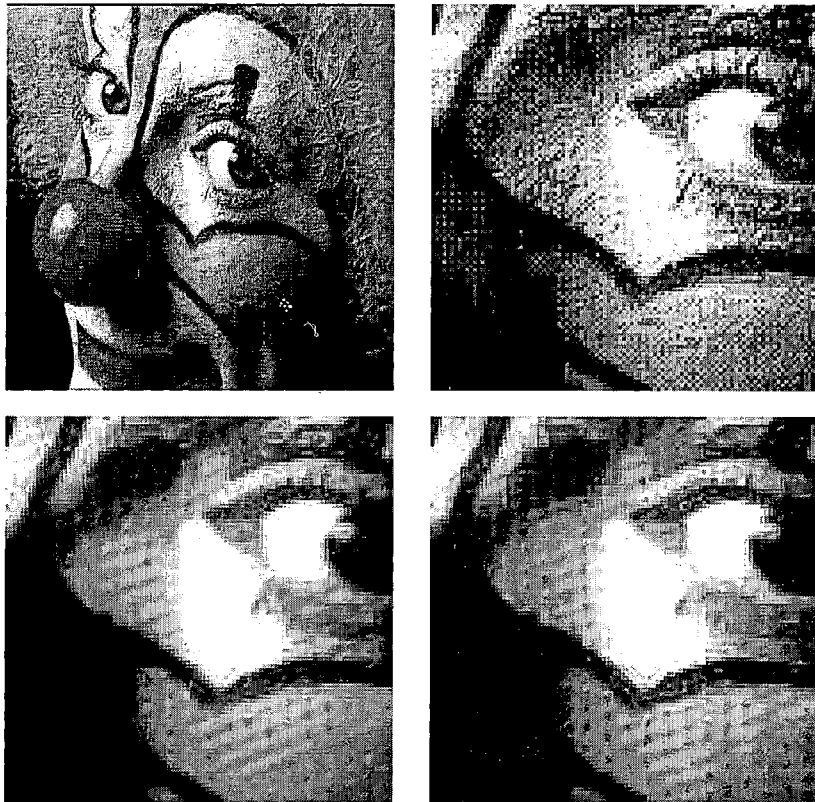


Figure 4: Top left: Original image. Top right: Relevant part of the image. Bottom left: Solution of (25) with  $m = 1$ ,  $\alpha = 0$  and  $\beta = 10$  (classical ROF setting) by Chambolle's algorithm applied to the dual quadratic problem with quadratic constraints. Bottom right: Solution of  $F(u) = \frac{1}{2}\|f - u\|_2^2 + \beta\|\mathcal{D}_1 u\|_1$  with the same parameters. This solution was computed by applying the ILOG CPLEX barrier Optimizer version 7.5 to the dual quadratic problem with linear constraints. The routine uses a modification of the primal-dual predictor-corrector interior point algorithm described in [14]. Due to the lack of rotation invariance vertical and horizontal directions are stressed .

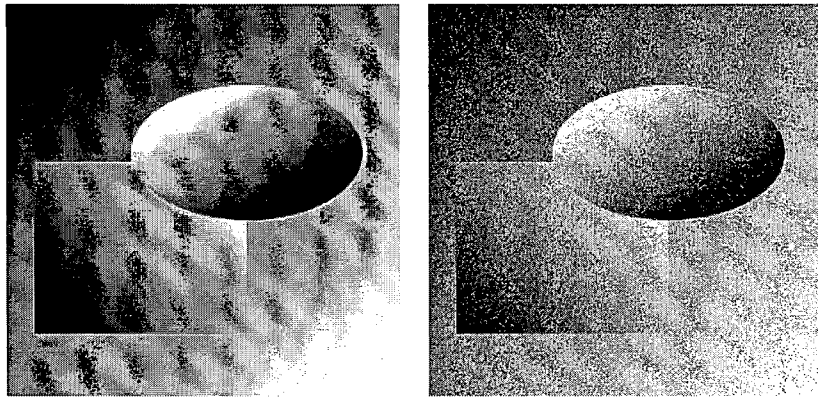


Figure 5: Denoising experiment in 2d. Left: Original image (size  $256 \times 256$ ). Right: Image with additive Gaussian noise, SNR 11.16.

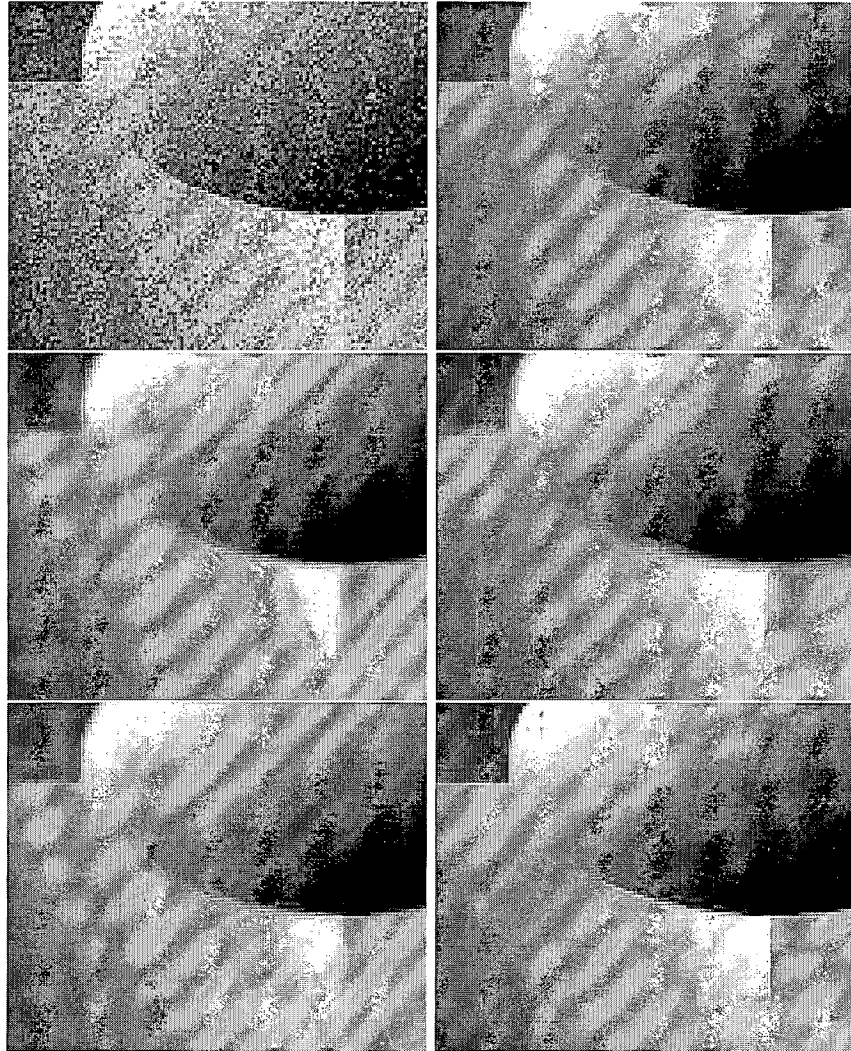


Figure 6: Denoising experiment in 2d. Sections with  $120 \times 100$  pixels of the resulting images. Top left: Noisy input image. Top right: Denoised image with ROF model. The staircasing effect is clearly visible. Middle: Denoising with second order model,  $m = 2$ ,  $\alpha = 0$ , left:  $\beta = 20$ , right:  $\beta = 50$ . No staircasing effect, but the edges are blurred. Bottom left: Denoising with second order model and gradient fitting term,  $m = 2$ ,  $\alpha = 1.2$ ,  $\beta = 50$ , yields better edge preservation. Bottom right: Second order model with gradient fitting term and Perona-Malik type diffusivity,  $m = 2$ ,  $\alpha = 1$ ,  $\beta = 1000$  with sharp edges and smooth grey value transitions.